fusional Models for Solid-Gas Reactions," *AIChE J.*, **14**, 311 (1968).
Kawahata, M., and P. L. Walker, Jr., "Mode of Porosity Development in Activated Anthracite," in *Proc. 5th Carbon Conf.*, **2**, 251-263, Pergamon, London (1962).
Kito, M., T. Onodera, and S. Sugiyama, *Kaguku Koguku* (Chem. Eng. Japan), **32**, 695 (1968); *Intern. Chem. Eng.*, **9**, 181 (1969).
Lacey, D. T., J. H. Bowen, K. S. Basden, "Theory of Noncatalytic Gas-Solid Reactions," *Ind. Eng. Chem. Fundamentals*, **4**, 275 (1965).
Lamond, T. G., and H. Marsh, "The Surface Properties of Carbon, III—The Process of Activation of Carbon," *Carbon*, **1**, 293 (1964).
Mendoza E., R. E. Cunningham, and J. J. Ronco, "Oxidation of Zinc Sulfide Pellets," *J. Catalysis*, **17**, 1, 194, 277 (1970).
Petersen, E. E., "Reaction of Porous Solids," *AIChE J.*, **3**, 443 (1957).
Rigg, T., "Hydrogen Reduction of the Chlorides of Bi-valent Chromium and Iron," *Can. J. Chem. Eng.*, **48**, 84 (1970).
Schechter, R. S., and J. L. Gidley, "The Change in Pore Size Distribution from Surface Reactions in Porous Media," *AIChE J.*, **15**, 339 (1969).
Scrivner, N. C., and F. S. Manning, "Reduction Kinetics of Swelling Wustite Particles," *ibid.*, **16**, 326 (1970).
Shen, J., and J. M. Smith, "Diffusional Effects in Gas-Solid Reactions," *Ind. Eng. Chem. Fundamentals*, **4**, 293 (1965).
Thomas, W. J., "The Effect of Oxidation on a Pore Structure of Some Graphitized Carbon Blacks," *Carbon*, **3**, 435 (1966).
Tsuchiya, H. M., A. G. Fredrickson, and R. Aris, "Dynamics of Microbial Cell Populations," in *Advances in Chem. Eng.*, **6**, 125, Academic Press, New York (1959).
Walker, P. L., Jr., Frank Rusinko, Jr., and L. G. Austin "Gas Reactions of Carbon" in *Advances in Catalysis*, **11**, 133, Academic Press, New York (1959).
Wen, C. Y., "Noncatalytic Heterogeneous Solid Fluid Reaction Models," *Ind. Eng. Chem.*, **160**, 34 (1968).
———., and L. Y. Wei, "Simultaneous Nonisothermal, Noncatalytic Solid-Gas Reactions," *AIChE J.*, **17**, 272 (1971).
Yagi, S., and D. Kunii in "5th Intern. Symp. on Combustion," 231, Reinhold, New York (1955).

Manuscript received April 2, 1971; revision received August 29, 1972; paper accepted October 13, 1972.

Gasification: Part II. Extension to Diffusion Control

Gasification model developed in Part I is extended to allow for mass transfer of oxidant to the particle and for intraparticle diffusion. For this extension, a moving boundary problem results which is solved numerically in conjunction with a two-point boundary value problem for the oxidant concentration profile in the particle. The extended model predicts, as expected, that mass transfer stifles gasification and intraparticle diffusion shifts gasification to the outer surface of the particle. For the conditions and parameters used in Part I, particle Thiele moduli above 10 result in particle shrinkage with negligible change in the solid properties, whereas if this modulus is less than 0.1, gasification is kinetically controlled.

KENJI HASHIMOTO and P. L. SILVESTON

University of Waterloo Waterloo, Ontario, Canada

SCOPE

In this portion we extend the gas-solid reaction model developed in Part I of this paper to cases where intraparticle diffusion must be considered. Our objectives in this extension are to further generalize the model, provide criteria which could be used to determine whether gasification is diffusionally or kinetically controlled, and finally to examine how mass transfer influences the development of solid properties with gasification.

Our model extension is applicable to systems where the physical properties of the solid undergoing gasification are important. An example is the partial gasification of chars to form activated carbon.

It is generally recognized that mass transfer is important in gas-solid reactions and it is taken into account in the shrinking core and homogeneous reaction models referred to in Part I. The approach followed in this paper to derive our model is similar to that used in the past as typified by Wen and co-workers (1963, 1968). Unlike Wen and others, a specific pore structure is considered. We assume a bidispersed pore size distribution in which the micropores account predominantly for surface area, porosity, and pore volume. The macropores serve as conduits carrying the oxidant and removing the gaseous products of the reaction. Our other assumptions are taken from Part I, for example, no ash remains after gasification so pore coalescence may occur and the particle size may change, micropores are uniform in length and cylindrical, and the gasification reaction is first-order in the oxidant.

Although we allow for enlargement of both micropore and macropores, micropores cannot become macropores and new pore initiation is limited to micropores.

Micropore shape is assumed not to change during gasification. The micropore size, therefore, is described by a mean pore radius and its change is related to gasification by measuring gasification as the flux of oxidant through the micropore mouth. This follows an approach suggested by Thomas (1966). Intraparticle diffusion of oxidant is handled through Fick's law using a variable effective diffusivity. Both Walker et al. (1959) and Wen (1963) before us have allowed the diffusivity to change during the reaction. Mass transfer to the particle is introduced conventionally as a boundary condition for the equation describ-

ing intraparticle diffusion. The coefficient, however, is allowed to vary with particle size. The pseudo stationary state assumption permitting the concentration gradients to be given by ordinary differential equations is employed for both micro and macropores.

An isothermal particle is assumed in our model. McGreavy and Cresswell (1970) have shown that particles can be treated as isothermal for most exothermic catalytic reactions, even when heats of reaction are large. However, they found that heat transfer to the particle was important for fast, highly exothermic reactions. Hills (1967, 1968) also finds heat transfer is important. However, heat transfer has not been allowed for in our treatment.

CONCLUSIONS AND SIGNIFICANCE

The gasification model derived in this work in terms of local moments and the local apparent density of the solid is given in Tables 1 and 2. Moments are related to the properties as shown in Table 1 of Part I. Because of the concentration gradients, the moments and solid properties vary radially. Integration, via Equation (31), must be used to express particle properties. Oxidant concentration appears in all equations of the model so the gradient must be determined at each instant to evaluate the local properties. Thus, the model entails solving Equations (25) to (27) which describes the diffusion of oxidant through the particle. Mathematically seen, a two-point boundary value problem must be solved. Since the particle itself shrinks as gasification proceeds, [Equation (30)], a moving boundary problem arises. The procedure of Murray and Landis (1959) was used to handle this complication.

Using as a basis the partial gasification of devolatilized anthracite considered in Part I, the influence of mass transfer on gasification was examined. Magnitude of the mass transfer resistances may be expressed by the Thiele moduli for the macro and micropores and the Sherwood number, all defined in terms of conditions at the start of the gas-solid reaction. Of these parameters, the macropore Thiele modulus seems the most important. If the macropore Thiele modulus is less than 0.1, gasification is kinetically controlled, whereas if the modulus is greater than 10, particle properties change negligibly with gasification and shrinkage alone occurs. In the latter case, the well known shrinking core model will satisfactorily describe the reaction. Within the Thiele modulus range indicated, increasing the modulus retards the overall rate of gasification and reduces the increase of specific surface area, volume and total pore numbers with extent of gasification. Figures 5 to 8 indicate quantitatively the influence of the modulus.

Conditions which lead to large micropore Thiele moduli will also result in large macropore moduli. Examined separately, large micropore moduli retard gasification but increase the importance of new pore initiation. The effect, as shown in Figure 8, is to increase the development of specific surface area with burn-off. Above a Sherwood number of 10, mass transfer to the particle surface can be neglected. Decreasing the Sherwood number below this value retards gasification.

These results are significant, in particular, for partial gasification of chars to make activated carbon. To achieve the largest increases of specific surface area, pore numbers, etc. with burn-off, gasification conditions should be chosen so that intraparticle diffusion of the oxidant is not important. Therefore, low temperatures and small particles should be employed. The macropore Thiele modulus provides a criteria for the choice of the proper conditions.

Investigation of the effect of the change of effective diffusivity with gasification indicates the effective diffusivity can be taken as a constant. Wen (1963) has reached the same conclusion. The small error this approximation introduces is greatly outweighed by the calculational simplification it provides.

BASIC MODEL

The population balance relation and its form in terms of moments, Equations (1) and (2) in Part I, hold for changing pore sizes regardless of the presence or absence of diffusional resistances.

To retain the relation of solid properties to moments of the pore size distribution as expressed in Table 1 of Part I, however, we must make the additional assumption that pore shape does not change during the gas-solid reaction. This is an awkward assumption in view of our kinetic model and the existence of concentration gradients in the pores. However, it is an assumption that has been made before (Thomas, 1966). Nonuniform pore growth has been treated by Peterson (1957), but the complications its use introduces are probably not justified by the added level of detail it provides.

Consideration of diffusion requires more information or assumptions about the solid structure than needed in Part I. Thus, in this paper, we deal with a bidispersed pore size distribution in which the micropore range contributes predominantly to the solid properties, such as surface area, porosity, etc. We further assume that micropores radiate from macropores and the latter pores act consequently as conduits bringing the gaseous reactant to the micropores where the bulk of the gas-solid reaction occurs. It is convenient for this system to treat diffusion in micro and macropores differently. For this reason, we will assume that the pore size density distribution function $f(r)$ refers only to micropores. Consequently, moments and thereby the properties related to the moments by Table 1 in Part I will refer to the micropores. As in Part I, the subscript i will be used to designate micropore properties or parameters. The subscript a will be used in our subsequent development for macropore properties or parameters.

We can now turn to gasification and proceed to develop a model specifically for this system.

ALLOWANCE FOR MICROPORE DIFFUSION

The difficulty introduced by pore shape change during gasification can be avoided by assuming the pore size distribution function is in terms of a mean pore radius $\overline{r}$.

Following Thomas (1966), the rate of gasification may be equated to the oxidant mass flow at the micropore mouth. This leads to

$$\frac{d\bar{r}}{dt} = -\frac{\bar{r} M_B}{2a \rho_t \bar{l}} \left(D_{ei} \frac{dc}{dz} \right)_{z=0} \tag{1}$$

Employing the kinetic assumption of Part I and the quasi steady state assumption that diffusion is rapid relative to the change of pore radius, the pore mouth gradient in Equation (1) may be found from the solution of

$$D_{ei} \frac{d^2c}{dz^2} - \frac{2 k_1 a c}{\bar{r}} = 0 \tag{2}$$

with $dc/dz = 0$ at $z = \bar{l}$ and $c = C$ at $z = 0$. This familiar equation may be readily solved. It is convenient, first of all, to normalize c, z, $\bar{r}$, and D_{ei} with C, the pore mouth concentration; r_0, the most probable radius for the distribution $f(\bar{r})$ at time zero; and D_{ei}^0, the effective micropore diffusivity for $\bar{r} = r_0$. If we assume that $D_{ei} = \delta D_K$, where δ is assumed to be invariant in gasification, then $D_{ei}/D_{ei}^0 = r^*$. r^* is the pore radius relative to r_0. The derivative in Equation (1) may be evaluated from the solution to Equation (2) giving

$$\frac{d\bar{r}}{dt} = \frac{k_1 M_B C}{\rho_t} \frac{\tanh(h_0/r^*)}{h_0/r^*} \tag{3}$$

where

$$h_0 = \bar{l} \sqrt{\frac{2 k_1 a}{r_0 \delta D_K^0}}$$

is the micropore Thiele modulus.

Substitution of Equation (3) in the $n < \bar{r}^{n-1} \frac{d\bar{r}}{dt} >$ term of the moment equation, Equation (2) in Part I, results in the expression

$$g_n = \frac{n k_1 M_B C}{\rho_t h_0 r_0} \int_0^\infty \bar{r}^n \tanh\left(\frac{r_0 h_0}{\bar{r}}\right) f(\bar{r})\, d\bar{r} \tag{4}$$

We show elsewhere (Hashimoto and Silveston, 1973b) that through the use of a mean value theorem g_n may be approximated closely by

$$g_n = \frac{n k_1 M_B C}{\rho_t} M_{n-1} e_n \tag{5}$$

e_n in Equation (5) may be treated as a pseudo effectiveness factor. When $n = 2$, e_n becomes the effectiveness factor defined by Equation (7).

Concentration gradients in the micropores do not change the birth and death contribution obtained in Part I. Substitution of these terms, derived in Part I, along with Equation (5), and expansion of the moment equation furnish the first three equations in Table 1.

The expression for the rate of change of apparent density on an inert matter free basis, Equation (20) in Part I, is altered somewhat by the presence of concentration gradients. The micropore contribution to the rate of gasification $\mathcal{R}_B$ may be expressed as

$$\mathcal{R}_{Bi} = \frac{\pi}{a} \int_0^\infty -D_{ei} \left(\frac{dc}{dz}\right)_{z=0} \bar{r}^2 f(\bar{r})\, d \tag{6}$$

Although the pore mouth concentration gradient can be expressed in terms of the micropore Thiele modulus as in Equation (3), it is convenient to introduce a micropore effectiveness factor (Mingle and Smith, 1961).

$$e_2 = \frac{\int_0^\infty -D_{ei} \left(\frac{dc}{dz}\right)_{z=0} \bar{r}^2 f(\bar{r})\, d\bar{r}}{2 k_1 a \bar{l} C \int_0^\infty \bar{r} f(\bar{r})\, d\bar{r}} \tag{7}$$

Making use of Equation (6) and introducing moments,

$$\mathcal{R}_{Bi} = 2\pi k_1 \bar{l} C e_2 M_1 \tag{8}$$

The contribution of pore initiation to $\mathcal{R}_B$ is unchanged from the term given in Part I as Equation (22), but since micro and macropores are treated separately a macropore contribution must be formulated. Assuming kinetics of gasification does not depend on pore size,

$$\mathcal{R}_{Ba} = k_1 \rho_B C S_a \tag{9}$$

where S_a is the specific macropore surface area.

Substituting for $\mathcal{R}_B$ leads to Equation (13) in Table 1. The set of equations permits calculation of solid properties at a point within a solid during gasification. From apparent density of the solid, local extent of gasification and/or porosity may be obtained. Equations (24) and (26) in Part I give the appropriate relations

Table 1. Gasification Model in Terms of Local Moments and Density

$$\frac{\partial M_0}{\partial t} - k_f \rho_B C + \phi \left(1 - \frac{\alpha}{2}\right) M_0^2 = 0 \tag{10}$$

$$\frac{\partial M_1}{\partial t} - \frac{k_1 M_B C}{\rho_t} e_1 M_0 - k_f \rho_B r_f C + \phi (1 - \alpha^2) M_0 M_1 = 0 \tag{11}$$

$$\frac{\partial M_2}{\partial t} - \frac{2 k_1 M_B C}{\rho_t} e_2 M_1 - k_f \rho_B r_f^2 C + \phi (1 - \alpha^3) M_0 M_2 - \phi \alpha^3 M_1^2 = 0 \tag{12}$$

$$\frac{\partial \rho_B}{\partial t} + \left(2\pi k_1 \bar{l} e_2 M_1 + k_1 \rho_B S_a + k_f \frac{\rho_B \rho_t}{M_B} \pi r_f^2 \bar{l} \right) C M_B = 0 \tag{13}$$

Making Equations (10) to (13) dimensionless by introducing the moments of $f(\bar{r})$ at $t = 0$, the relations in Table 1 of Part I, the initial values of the solid properties, and $\tau = k_1 C_g M_B S_i^0 t$, we obtain the equations in Table 2 in terms of the coefficients b defined in Table 2 of Part I. However, b_{70} and b_{80} contain ϕ_∞ rather than ϕ and are constants. Allowance for diffusion appears through the presence of ψ, the normalized oxidant concentration in the macropores, in most terms and e_1 in Equation (15) and e_2 in Equation (16). The σ in Equation (17) is now defined as

$$\sigma = \frac{S_a^0}{S_i^0} + \frac{\pi k_f \rho_t \bar{l} r_f^2}{k_1 M_B S_i^0}$$

Table 2. Gasification Model in Terms of Dimensionless Variables and Parameters

$$\frac{\partial \mu_0}{\partial \tau} - b_1 \psi \rho_B^* + b_{70} \left(1 - \frac{\alpha}{2}\right) \phi^* \mu_0^2 = 0 \tag{14}$$

$$\frac{\partial \mu_1}{\partial \tau} - b_2 e_1 \psi \mu_0 - b_3 \psi \rho_B^* + b_{70} (1 - \alpha^2) \phi^* \mu_0 \mu_1 = 0 \tag{15}$$

$$\frac{\partial \mu_2}{\partial \tau} - b_4 e_2 \psi \mu_1 - b_5 \psi \rho_B^* - b_{80} \alpha^3 \phi^* \mu_1^2 + b_{70} (1 - \alpha^3) \phi^* \mu_0 \mu_2 = 0 \tag{16}$$

$$\frac{\partial \rho_B^*}{\partial \tau} + \psi (e_2 \mu_1 + \sigma \rho_B^*) = 0 \tag{17}$$

ALLOWANCE FOR MACROPORE DIFFUSION AND MASS TRANSFER TO PARTICLE SURFACE

Assumptions about macropore length, shape, and location of intersections may be avoided by introducing the effective diffusivity of the solid instead of considering a single pore as in the micropore case. Employing the quasi stationary state assumption shown to be justified in most situations by Bischoff (1963) and Wen (1963), a material balance on the oxidant in the solid (Aris, 1965; Petersen, 1965),

$$\frac{d}{dR}\left(D_e R^2 \frac{dC}{dR}\right) - (1-\theta_I) R^2 \mathcal{R}_A = 0 \quad (18)$$

where D_e is the local effective diffusivity of the porous solid, θ_I is the volume fraction of the inert, and $\mathcal{R}_A$ is the rate of oxidant consumption through gasification. For a gasification reaction $aA(g) + B(s) \rightarrow P$ where B is solid and A is oxidant, $\mathcal{R}_A = a\mathcal{R}_B$.

The boundary conditions for Equation (18) are

$$R = 0: \quad \frac{dC}{dR} = 0 \quad (19)$$

$$R = R_s: \quad k_g (C_g - C_s) = k_1 a\, \theta_B{}^0\, \rho_{B_s}{}^*\, C_s + \left(D_e \frac{dC}{dR}\right)_{R=R_s} \quad (20)$$

Equation (20) allows for mass transfer of oxidant through the boundary layer to the particle surface and reaction at the surface. The group $(\theta_B{}^0\, \rho_B{}^*)$ is the reactive fraction of the external surface. Equation (18) describes a linear two-point boundary value problem with variable coefficients.

The effective diffusivity may vary with the extent of gasification. Since we have bypassed a macropore shape and intersection model, an empirical relation must be used to relate D_e to solid properties. We follow Wen (1963) who assumes effective diffusivity is proportional to the porosity taken to an exponent β. A dimensionless effective diffusivity is then

$$\mathcal{D} = (\theta^*)^\beta = \left[1 + \frac{\theta_B{}^0}{\theta^0}(1 - \rho_B{}^*)\right]^\beta \quad (21)$$

The initial volume fractions θ^0, $\theta_B{}^0$ are calculated from the inert density ρ_I, the weight fraction of inerts in the carbon ω_I, the initial apparent density (including inert matter) ρ_0, and the true density of the gasifiable solid ρ_t. The relations are

$$\theta_B{}^0 = \frac{\rho_0}{\rho_t}(1 - \omega_I) \quad (22)$$

$$\theta^0 = 1 - \rho_0\left(\frac{\omega_I}{\rho_I} + \frac{1-\omega_I}{\rho_t}\right) \quad (23)$$

Correlations for mass transfer to particles generally show the Sherwood number to be an exponential function of the particle Reynolds number. The mass transfer coefficient, therefore, will depend on particle size so that

$$k_g = k_g{}^0\, \xi_s{}^{-\epsilon} \quad (24)$$

where $k_g{}^0$ is the coefficient at R_0 and ϵ is an appropriate exponent.

Introducing the expression for $\mathcal{R}_A$ and rendering Equations (18) to (20) dimensionless using the bulk oxidant concentration C_g and the initial properties of the solid

$$\frac{1}{\xi^2}\frac{d}{d\xi}\left(\mathcal{D}\,\xi^2 \frac{d\psi}{d\xi}\right) - H_0{}^2 (e_2 \mu_1 + \sigma\, \rho_B{}^*)\psi = 0 \quad (25)$$

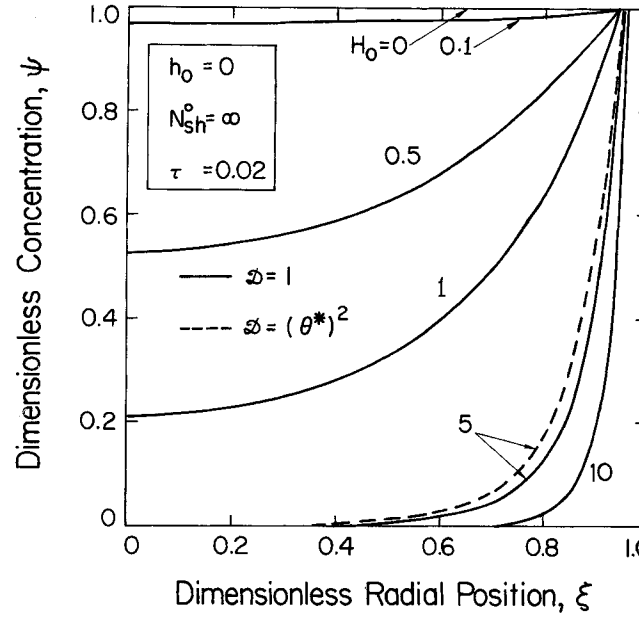

Fig. 1. Concentration profile of oxidant in porous carbon particle at $\tau = 0.02$.

with

$$\xi = 0: \quad \frac{d\psi}{d\xi} = 0 \quad (26)$$

$$\xi = \xi_s: \quad \frac{d\psi}{d\xi} = N_{Sh}{}^0 \frac{\xi_s{}^{-\epsilon}}{\mathcal{D}_s}\left[1 - \left(1 + \lambda \frac{\rho_{B_s}{}^*}{\xi_s{}^{-\epsilon}}\right)\psi_s\right] \quad (27)$$

where ξ is the relative radial position assuming a spherical particle, $N_{Sh}{}^0$ is the Sherwood number at $t = 0$ and λ is a constant containing the ratio of gasification rate constant to mass transfer coefficient. The initial properties in Equation (25) are gathered in a particle Thiele modulus

$$H_0 = R_0 \sqrt{\frac{k_1 a\, \rho_B{}^0\, S_i{}^0\, \theta_B{}^0}{D_e{}^0}}$$

If we neglect the change in effective diffusivity and the mass transfer coefficient with gasification, the $\mathcal{D}_s$ and ξ_s in the right-hand side of Equation (27) drop out.

The influence of mass transfer on the overall reaction is usually represented by a particle effectiveness factor. For gasification, this factor may be defined as

$$E_{tp} = \frac{k_1 a\, \theta_B{}^0\, \rho_{B_s}{}^*\, C_s\, R_s{}^2 + \int_0^{R_s} \mathcal{R}_A (1-\theta_I) R^2\, dR}{k_1 a\, \theta_B{}^0\, \rho_{B_s}{}^*\, C_g\, R_s{}^2 + \int_0^{R_s} \mathcal{R}_{A_g} (1-\theta_I) R^2\, dR} = \frac{\zeta\, \rho_{B_s}{}^*\, \psi_s\, \xi_s{}^2 + \int_0^{\xi_s} (e_2\mu_1 + \sigma\rho_B{}^*)\xi^2\psi d\xi}{\zeta\, \rho_{B_s}{}^*\, \xi_s{}^2 + \int_0^{\xi_s} (\mu_1 + \sigma\rho_B{}^*)\xi^2 d\xi} \quad (28)$$

and interpreted as the ratio of the gasification rate at any extent of gasification to the rate which would be found if concentration gradients were absent in the solid. E_{tp} allows for gasification at the external surface of the particle. However, the surface terms can be neglected unless the porosity is very low. In the later stages of gasification E_{tp} will approach unity (see Figure 2).

The complex change in rate due to shrinkage, mass transfer, and changing surface area and porosity is also

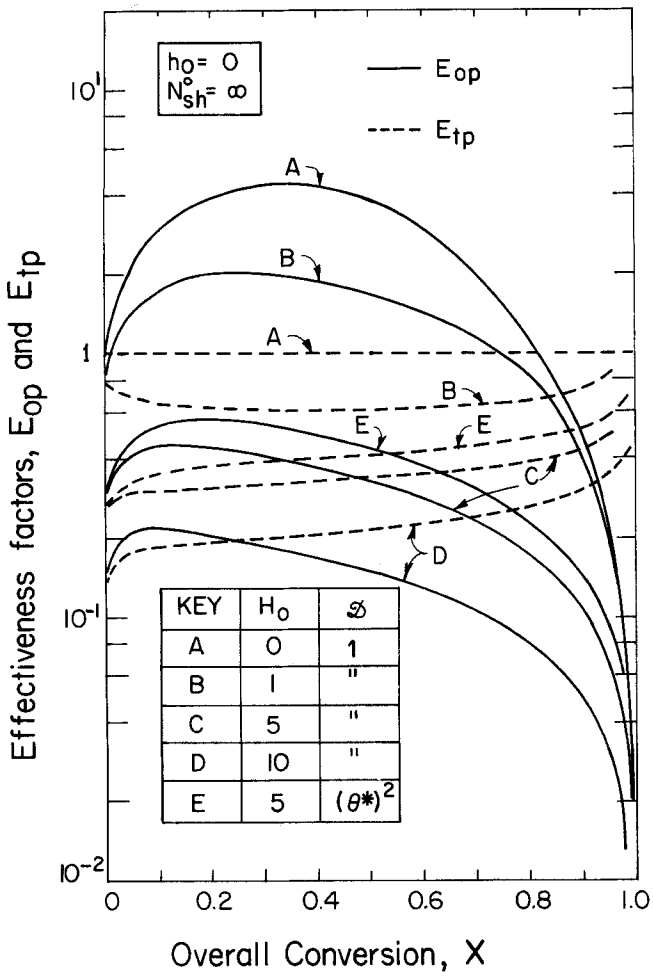

Fig. 2. Particle effectiveness factors as functions of burn-off and diffusional resistance.

of interest. This may be represented by a second type of effectiveness factor which is the ratio of the actual gasification rate at any time to the rate for the original particle at $t = 0$ neglecting mass transfer resistance

$$E_{0p} = \frac{k_1 a\, \theta_B{}^0\, \rho_{Bs}{}^*\, C_s\, R_s{}^2 + \int_0^{R_s} \mathcal{R}_A\,(1-\theta_I)\, R^2\, dR}{k_1 a\, \theta_B{}^0\, C_g\, R_0{}^2 + \frac{1}{3}(1-\theta_I)\, \mathcal{R}_{Ag}{}^0\, R_0{}^3}$$

$$= \frac{\zeta\, \rho_{Bs}{}^*\, \psi_s\, \xi_s{}^2 + \int_0^{\xi_s} (e_2\, \mu_1 + \sigma \rho_B{}^*)\, \xi^2 \psi\, d\xi}{\zeta + (1+\sigma)/3} \qquad (29)$$

In contrast to E_{tp}, E_{0p} may be greater than one but it decreases rapidly in the last stages of gasification and eventually falls to zero as the particle is totally consumed.

The possibility of a mass transfer resistance at the particle surface introduces a C_s, the oxidant surface concentration, in the particle shrinkage equation [Equation (27) in Part I]. Made dimensionless, the shrinkage equation becomes

$$\frac{d\xi_s}{d\tau} + b_6 \psi_s = 0 \qquad (30)$$

Local variations of solid properties due to the oxidant concentration gradient in the particle makes integration necessary to obtain the mean properties. The mean moments are given by

$$\bar{\mu}_n = \frac{3}{\xi_s{}^3} \int_0^{\xi_s} \mu_n\, \xi^2\, d\xi \qquad (31)$$

The mean apparent density $\bar{\rho}_B{}^*$ may be obtained by replacing μ_n with $\rho_B{}^*$. Relative porosity depends only on the apparent density [Equation (26) in Part I] so

$$\bar{\theta}^* = 1 + \frac{\theta_B{}^0}{\theta^0}(1 - \bar{\rho}_B{}^*) \qquad (32)$$

The burn-off X, defined by Equation (25) in Part I, becomes

$$X = 1 - \bar{\rho}_B{}^*\, \xi_s{}^3 \qquad (33)$$

Gasification of the particle interior neglecting shrinkage is given by $1 - \bar{\rho}_B{}^*$. Mean relative micropore properties $\bar{\Lambda}_i$, $\bar{\Gamma}_i$, $\bar{\Omega}_i$, $\bar{\gamma}_e$, may be found using the expressions in Table 1 of Part I by replacing μ_n and $\rho_B{}^*$ by their means $\bar{\mu}_n$ and $\bar{\rho}_B{}^*$ and changing the subscript. Values relative to the mass of original solid may be obtained by multiplying the expressions by $1 - X$.

The gasification model modified for mass transfer consists of the equations in Table 2, Equations (25) and (30), and the relations given in the last two paragraphs. The equations in Table 2 are nonlinear, coupled through ψ, $\rho_B{}^*$ and μ_n, and Equation (25) is a two-point boundary value problem so that we must resort to fairly tedious numerical integration to evaluate the change in properties. The coupling of shrinkage and the oxidant concentration through Equations (27) and (30) introduce a moving boundary to complicate the numerical solution.

ALLOWANCE FOR THE MOVING BOUNDARY

Bankoff (1964) catalogues a variety of methods, most of which involve a transformation which immobilizes the boundary. We have employed one of these due to Murray and Landis (1959). These authors propose a transformation akin to that from an Eulerian to a Lagrangian coordinate system. If s is a scalar, such as μ_0, and a function of both dimensionless time and radial position, the rate of change of s at an interior point i, allowing for both contributions will be

$$\left(\frac{ds}{d\tau}\right)_i = \left(\frac{\partial s}{\partial \tau}\right)_i + \left(\frac{\partial s}{\partial \xi}\right)_i \frac{d\xi_i}{d\tau} \qquad (34)$$

Since $d\xi_s/d\tau$ [Equation (30)] not $d\xi_i/d\tau$ is available, a more convenient form of Equation (34) is

$$\left(\frac{ds}{d\tau}\right)_i = \left(\frac{\partial s}{\partial \tau}\right)_i + \frac{\xi_i}{\xi_s}\left(\frac{\partial s}{\partial \xi}\right)_i \frac{d\xi_s}{d\tau} \qquad (35)$$

Use of this transformation allows us to solve a system of ordinary differential equations. For example, let $s = \mu_0$. Then, the $(\partial s/\partial \tau)_i$ of Equation (35) may be replaced by Equation (14), and $d\xi_s/d\tau$ by Equation (30) to yield

$$\frac{d\mu_{0,i}}{d\tau} = b_1 \psi_i\, \rho_{Bi}{}^* - b_{7_0}\left(1 - \frac{\alpha}{2}\right)\phi_i(\mu_{0,i})^2 - \frac{b_6 \psi_s \xi_i}{\xi_s}\left(\frac{\partial \mu_0}{\partial \xi}\right)_i \qquad (36)$$

Similar equations may be obtained for μ_1, μ_2, and $\rho_B{}^*$. Equation (25) does not change, however. Equation (35) applies to the oxidant concentration. Since $(\partial \psi/\partial t)_i = 0$, it becomes

$$\left(\frac{d\psi}{d\tau}\right)_i = \frac{\xi_i}{\xi_s}\left(\frac{\partial \psi}{\partial \xi}\right)_i \frac{d\xi_s}{d\tau} \qquad (37)$$

and may be used to predict the change in oxidant concen-

tration over each time step. The system of equations obtained by the transformation lend themselves well to conventional numerical methods.

NUMERICAL SOLUTION

Partial derivatives with respect to ξ, as shown in Equations (36) or (37), were approximated by central differences leading to $NS + 1$ equations for each moment, for apparent density, for particle radius and for the oxidant concentration where NS is the number of radial increments chosen. At the center of the particle, the $\partial\mu_n/\partial\xi$ term vanishes because of symmetry. At the particle surface the central difference approximation is not suitable and a three point Lagrangian difference may be used:

$$\left(\frac{\partial\mu_n}{\partial\xi}\right)_s = \frac{1}{2\Delta\xi}\left(\mu_{n,s-2} - 4\mu_{n,s-1} + 3\mu_{n,s}\right) \quad (38)$$

This approximation is of the same order as the central difference. The set of equations resulting from these approximations are given in a detailed manuscript available from the authors.

Integration of the set of $\{5(NS + 1) + 1\}$ equations in dimensionless time τ was accomplished with a second-order Runge-Kutta-Gill procedure. At each time step in the integration of the density and moment equations, the concentration distribution within the particle was determined. To accomplish this, a central difference approximation was used for Equation (25). Boundary conditions, Equations (26) and (27), were used to establish the approximations at $i = 0$ and $i = s$. Separate sets of equations were developed assuming variable D_e and then constant D_e. Both sets of equations are given in the detailed manuscript referred to above. The sets of equations are linear in ψ and were solved through their matrix representation

$$\mathbf{A} \cdot \boldsymbol{\Psi} = \mathbf{B} \quad (39)$$

where $\boldsymbol{\Psi}$ is the vector of normalized concentration in the particle, $\mathbf{B}$ is a vector containing only one nonzero element (contributed by $i = s$), and $\mathbf{A}$ is a tridiagonal coefficient matrix of dimension $NS + 1$. The Thomas method of direct elimination was used. $\mathbf{A}$ and $\mathbf{B}$ were evaluated using parameters of the previous time step.

Initially, an oxidant concentration gradient was assumed to exist in the particle. It was calculated from an analytical expression obtained from setting all the dimensionless variables in Equations (25) to (27) except ψ to unity so they became

$$\frac{1}{\xi^2}\frac{d}{d\xi}\left(\xi^2\frac{d\psi^0}{d\xi}\right) - \Lambda^2\psi^0 = 0 \quad (40)$$

where

$$\Lambda = H_0\sqrt{e_2^0 + \sigma}$$

and

$$\xi = 0 : \frac{d\psi^0}{d\xi} = 0 \quad (41)$$

$$\xi = 1 : \frac{d\psi^0}{d\xi} = N_{Sh}^0\left(1 - (1 + \lambda)\psi_s^0\right) \quad (42)$$

The micropore effectiveness factor e_2^0 is independent of ψ^0 so Equation (40) is linear. Its solution is

$$\psi^0 = \frac{\sinh(\xi\Lambda)}{\gamma\,\xi\,\sinh\Lambda} \quad (43)$$

where $\gamma = 1 + \lambda + 1/N_{Sh}^0\,(\Lambda\coth\Lambda - 1)$. The two effectiveness factors E_{tp} and E_{0p} are equal and may be written as

$$E_{tp}^0 = E_{0p}^0 = \frac{\dfrac{3(e_2^0 + \sigma)}{\gamma\Lambda(1 + \sigma)}\left[\dfrac{1}{\tanh\Lambda} - \dfrac{1}{\Lambda}\right] + \dfrac{3\xi}{(1 + \sigma)}\left[\dfrac{\Lambda}{\sinh\Lambda}\right]}{1 + \dfrac{3\xi}{(1 + \sigma)}} \quad (44)$$

For the usual case of $S_i^0 >> S_a^0$, a satisfactory approximation is

$$E_{tp}^0 = E_{0p}^0 = \frac{3(e_2^0 + \sigma)}{\gamma\Lambda(1 + \sigma)}\left[\frac{1}{\tanh\Lambda} - \frac{1}{\Lambda}\right] \quad (45)$$

Effectiveness factors E_{tp} and E_{0p} other than at $\tau = 0$ were evaluated from Equations (28) and (29) using Simpson's rule. This formula was also employed to evaluate $\overline{\mu_n}$, $\overline{\rho}^*$ from the $NS + 1$ local values. The mean relative moments and apparent density were used in turn to calculate the particle properties and burn-off.

Convergence of the computing scheme outlined above was studied for the ranges $10 < NS < 50$ and $5 \times 10^{-4} < \Delta\tau < 2 \times 10^{-3}$ and found to be sensitive to NS primarily. For $H_0 = 1$ and $h_0 = 10^{-5}$, $NS = 10$ was satisfactory, whereas for $5 < H_0 < 10$, $h_0 = 5$, at least $NS = 20$ must be used. To reduce programming the calculations for Part I were performed by setting H_0 and h_0 to 10^{-5}, thereby neglecting the concentration gradients. It was found that for these values $NS = 4$ gave satisfactory convergence. In all calculations, $\Delta\tau = 2 \times 10^{-3}$ was used and reducing $\Delta\tau$ produced only slight improvement in the convergence. About 50 time steps were required for burn-off of the order of 95% when gradients were neglected.

The program, written in WATFIV required about 2.8×10^{-3} seconds per radial increment or 0.014 sec/time step at $NS = 4$ on the University of Waterloo's IBM 360-75.

CONSEQUENCE OF MASS TRANSFER LIMITATIONS

The effects of mass transfer will be examined for the system considered in Part I—the gasification of devolatilized anthracite with CO_2 (Kawahata and Walker, 1962).

The dimensionless oxidant concentration profile is calculated for each time step in the numerical procedure just described. Profiles after 10 steps when $\tau = 0.02$ is shown in Figure 1 for H_0 ranging from 0 to 10. Micropore diffusion is considered unimportant ($h_0 \cong 0$) and mass transfer to the particle surface is taken as rapid ($N_{Sh} \cong \infty$). The concentration remains essentially uniform through the particle at $H_0 = 0.1$ but an appreciable gradient appears at $H_0 = 0.5$. At $H_0 = 5$, the gasification occurs essentially only in the zone $0.8 < \xi < 1.0$, while above $H_0 = 10$, gasification occurs only on the surface of the particle which is to all intents nonporous. Surface gasification for $H_0 > 5$ is also illustrated in Figures 6 to 8 which show virtually no change in the solid properties with gasification.

Effectiveness factors indicate the magnitude of concentration gradients so that the effect of the Thiele modulus, burn-off, and other variables on the gradient can be examined conveniently in effectiveness factor plots. Figures 2 and 3 plot the transient effectiveness factor, E_{tp} [Equation (28)], and the second type based on initial conditions E_{0p} [Equation (29)], versus burn-off X. At $H_0 = 0$ (curve "A" in Figure 2) E_{tp} is constant at one, but E_{0p} goes through a maximum reaching about 4 before decreasing to zero as gasification approaches completion. The rapid increase of surface area and thus gasification rate with X

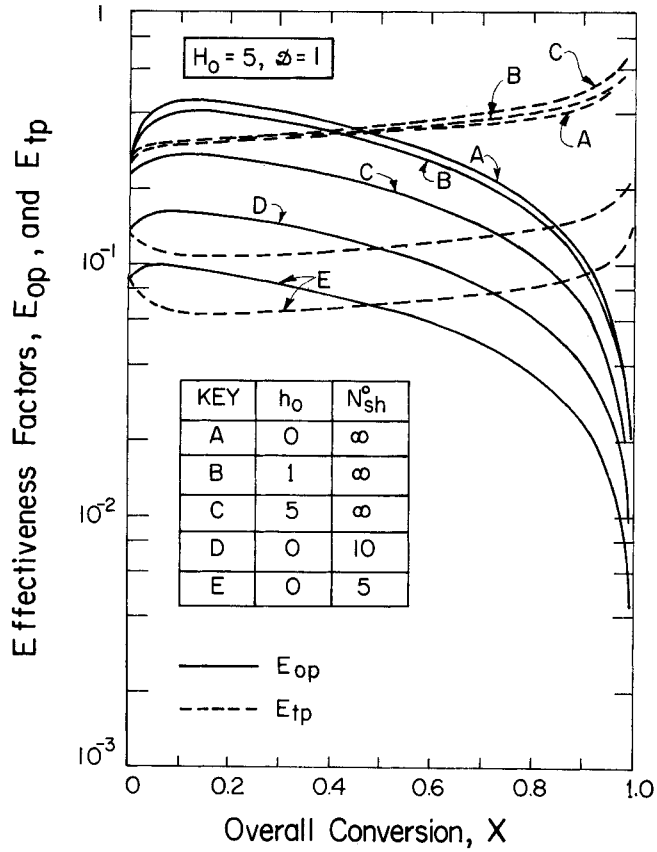

Fig. 3. Influence of micro pore diffusional resistance and mass transfer rate to the particle surface on particle effectiveness factors.

is responsible for this maximum. The B curves for $H_0 = 1$ show a maximum in E_{0p} and a flat minimum in E_{tp} attributable to increasing surface area. The upturn of E_{tp} at $X \rightarrow 0$ and $X \rightarrow 1$ results from a flattening of the concentration profile. The C and D curves in Figure 2 show the expected large influence of H_0 on the effectiveness factors. E_{tp} continuously increases with X and does not exhibit a minimum. This indicates the decrease in radius is compensating for surface increases at low τ. The maximum in E_{0p} also becomes much smaller suggesting again that very little increase of surface occurs in gasification above $H_0 = 5$.

The effect of the micropore diffusion in terms of the micropore Thiele modulus h_0 and mass transfer to the surface, as the Sherwood number $N_{Sh}{}^0$ are illustrated in Figure 3 for $H_0 = 5$. h_0 has only a small effect on E_{tp} and E_{0p} below $h_0 = 5$, as may be seen by comparing curves A, B, and C. Even at $h_0 = 5$, micropore diffusion is much less important than diffusion in the macropore structure for the devolatilized anthracite system. Only if micropore lengths are very long compared to pore radii could transport in the micropores become important. High temperatures which could cause $h_0 > 1$ will also sharply increase H_0 resulting in gasification only at the outer surface of the particle.

Curves A, D, E indicate the influence of mass transfer to the particle on E_{tp} and E_{0p}. The effect of decreasing $N_{Sh}{}^0$ to 10 on E_{tp} or E_{0p} is much greater than letting $h_0 = 5$. When $N_{Sh}{}^0 = 5$, a condition where surface transport is a dominant step, E_{tp} and E_{0p} drop about 5-fold from the $N_{Sh}{}^0 = \infty$ case. The drop is about as great as caused by increasing H_0 from 1 to 10. Thus, mass transfer to the surface is an important consideration. At $N_{Sh}{}^0 = 10$ (curve D), the maximum in E_{0p} has virtually disappeared indicating that at moderate H_0 and low $N_{Sh}{}^0$ surface area does not increase and gasification results only in size reduction.

Figures 4 through 8 illustrate aspects of the influence of intraparticle diffusion on the course of gasification and the change of properties. An important effect of intraparticle diffusion is to slow down gasification. This effect is illustrated in Figure 4 which plots the overall conversion X against dimensionless time τ. For $H_0 = 0$, $X = 0.2$ at $\tau = 0.013$, whereas for the same burn-off at $H_0 = 1$, $\tau = 0.016$ while at $H_0 = 10$, $\tau = 0.031$.

Figure 5 shows the variation of dimensionless particle radius ξ_s with X and illustrates again that diffusional resistance favors particle shrinkage. A plot of ξ_s versus τ, however, results in a single curve for all H_0, since ξ_s is controlled by a constant b_6 and ψ_s [Equation (30)] which

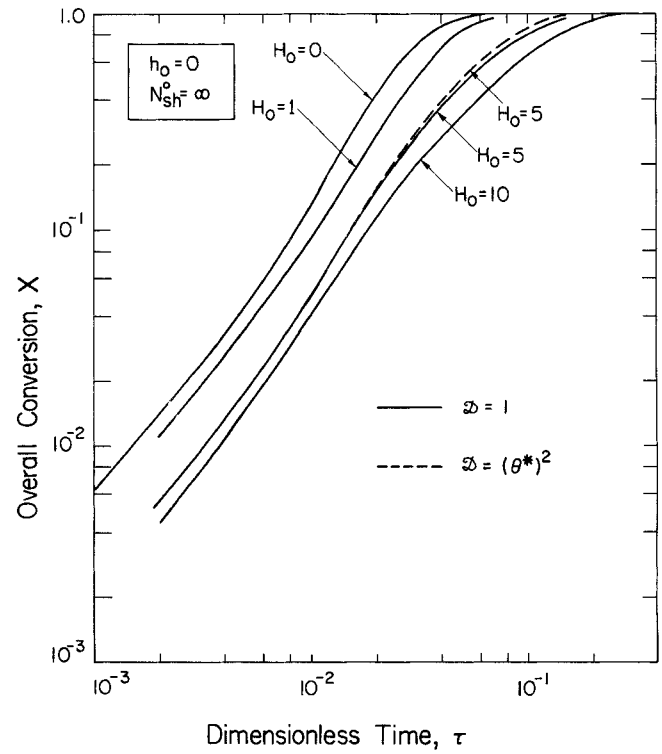

Fig. 4. Burn-off as a function of gasification time and diffusional resistance.

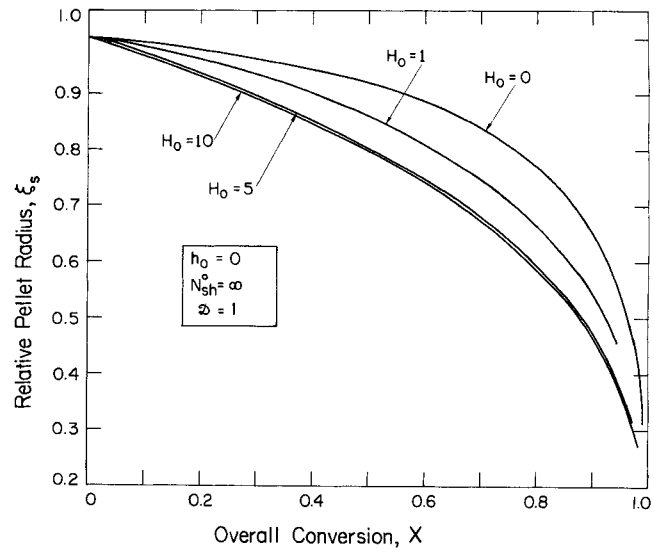

Fig. 5. Particle shrinkage as a function of burn-off and diffusional resistance.

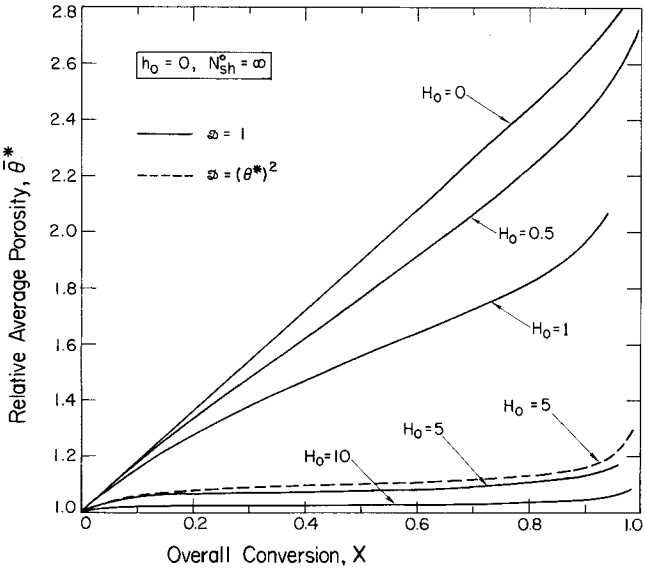

Fig. 6. Particle relative porosity as a function of burn-off and diffusional resistance.

is independent of H_0.

Figure 6 plots average relative porosity $\overline{\theta}^*$ against X for various levels of diffusional resistance. The figure shows virtually no increase in $\overline{\theta}^*$ above $H_0 = 5$. Porosity thus changes little when intraparticle diffusion of the oxidant controls gasification. In contrast, when gasification is kinetically controlled, $\overline{\theta}^*$ increases almost proportionally with X. Figure 7 shows the effect of diffusion on the change in mean relative pore radius with conversion. Particle Thiele moduli greater than 1, suppress the increase in pore size. Above $H_0 = 5$, there is virtually no change in $\overline{\gamma}_e$ with X. The shape of the curve at $H_0 = 0$ is interpreted in Part I.

Only a small increase of surface occurs during gasification in the presence of intraparticle diffusion. At $H_0 = 5$ and $X = 0.5$ in Figure 8, $\overline{\Gamma}_i \cong 5$, while at $H_0 = 10$, $\overline{\Gamma}_i \cong 3$ compared with $\overline{\Gamma}_i \cong 30$ for $H_0 = 0$. The significant maximum in $\overline{\Gamma}_i$ for $H_0 = 0$, caused by competition between new pore initiation and pore coalescence (discussed in Part I), occurs for $H_0 > 1$, but at high burn-off. The dashed curve for $h_0 = 5$ shows appreciably more surface development than the case shown where micropore diffusion may be neglected ($h_0 = 0$). This arises because micropore diffusional resistance reduces pore growth but does not effect new pore initiation. The latter, however, increases surface much more than pore growth in our model.

The absorption capacity of activated carbons is closely associated with specific surface, porosity, and mean pore diameter. The model results discussed in the last few paragraphs suggest that processes for the activation of chars by partial gasification using steam or CO_2 should be designed to avoid transport resistances. Low temperatures and as small particle sizes as feasible should be used.

Our model also suggest that where diffusional resistances are large, the shrinking core model will describe gasification satisfactorily. Of course, when this model is applicable, the solid properties in the core will be those of the original solid.

Results discussed so far assume constant effective diffusivity ($\mathfrak{D} = 1$). The dashed lines in Figures 1, 4, and 6 to 8 show the effect of making effective diffusivity a function of porosity [Equation (21)]. Choice of $\beta = 2$ for the exponent was based on Walker et al. (1959) observations with carbon rods. Results for variable D_e in all figures are for $H_0 = 5$, because for $H_0 < 1$, intraparticle diffusion is unimportant, while at $H_0 = 10$ gasification is confined to the outer surface so that the diffusivity has little effect. It is clear from these figures that allowing D_e to vary with porosity changes the behavior of the gasification model only slightly. Variable D_e does have a larger influence on the effectiveness factors. Comparing curves C and E in Figure 2 shows constant D_e introduces an error of the order of 25% at $H_0 = 5$. Allowiing for a variable effective diffusivity, however, remains a second-order consideration. Wen (1963) reached the same conclusion for his gas-solid reaction model. Simplification of the model that is achieved for a constant D_e thus seems to be amply justified by the small error a constant D_e introduces.

In this last section, we have chosen to examine the influence of mass transfer only through the Thiele moduli and N_{Sh}^0. An alternate approach would be to compare the behavior of systems with different particle sizes, initial mean pore diameters, or pore size distributions or for different temperatures whereby mass transfer is important in one system but not in the other. For a given material, H_0 depends upon a number of parameters such as R_0. However, the initial particle radius also appears in b_6. Thus, if changing particle size increases H_0 and N_{Sh}^0, b_6 will decrease proportionally. If temperature causes the H_0 change, b_7 and b_8 will change and perhaps b_1, b_3 and b_5 as well. All coefficients except b_4 depend on S_i^0, but this property of r_0 enters into the values of H_0 and h_0. In our study, of course, we have held b_i's constant while varying H_0, N_{Sh}^0 and h_0.

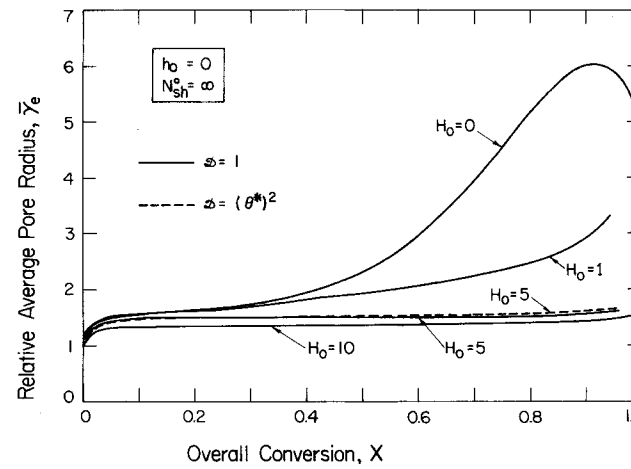

Fig. 7. Particle relative pore radius as a function of burn-off and diffusional resistance.

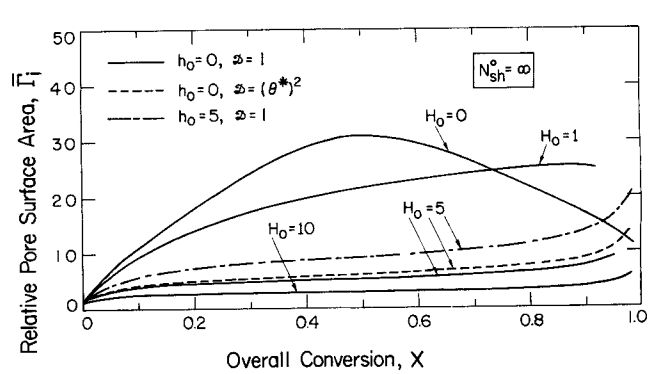

Fig. 8. Particle surface area as a function of burn-off and diffusional resistance.

ACKNOWLEDGMENTS

Support from a Water Resources Research grant of the Canadian Department of Energy, Mines and Resources, from the Faculty of Engineering, University of Waterloo, and the Japanese Ministry of Education is most gratefully acknowledged. Helpful discussions of our work were held with K. S. Chang (Waterloo), H. M. Hulburt (Northwestern) and P. L. Walker, Jr., (Penn State).

NOTATION

A, $\mathbf{A}$ = oxidant, coefficient matrix [Equation (39)]
a = stoichiometric constant
B, $\mathbf{B}$ = reactive solid, vector [Equation (39)]
b_i = dimensionless group of parameters (see Table 2, Part I)
C = macropore oxidant concentration
c = micropore oxidant concentration
D_e, D_{ei} = effective diffusivity in the solid, in the micropore
D_K = Knudsen diffusivity
E_{0p} = particle rate ratio [Equation (29)]
E_{tp} = particle effectiveness factor [Equation (28)]
e_n = micropore pseudo effectiveness factor
e_2 = micropore effectiveness factor [Equation (7)]
$f(\bar{r})$ = micropore size probability density function
g_n = pore growth term $= n < \bar{r}^{n-1}\, d\bar{r}/dt >$
H_0 = particle Thiele modulus $= R_0 \sqrt{\dfrac{k_1\, a\, \rho_B{}^0\, S_i{}^0\, \theta_B{}^0}{D_e{}^0}}$
h_0 = micropore Thiele modulus $= \bar{l} \sqrt{\dfrac{2k_1\, a}{r_0\, \delta D_K{}^0}}$
k_f = rate coefficient for pore initiation
k_g = mass transfer coefficient for oxidant
k_1 = gasification rate coefficient
M_B = molecular weight of the solid reactant (carbon)
M_n = nth moment about the origin $= \int_0^\infty (\bar{r})^n f(\bar{r})\, d\bar{r}$
NS = number of radial increments
n = integer, usually an exponent
N_{Sh} = modified Sherwood number $= \dfrac{k_g R_s}{D_e}$
R = radial dimension of solid particle
R_0 = initial particle radius
R_s = radius of particle
r = pore radius, micropore radius
r_f = radius of new pore (See Part I)
$\bar{r}$ = mean micropore radius
r_0 = initial mean pore radius
S = specific pore surface area
s = scalar property
t = time
X = overall extent of gasification or burn-off
z = axial dimension in micropore
α = pore radius combination coefficient (see Part I)
β = exponent for variable diffusivity
Γ_i = relative mean micropore surface area
γ = parameter in Equation (43)
ζ = parameter in Equations (28) and (29) $= \dfrac{1}{R_0 \rho_t S_i{}^0}$
γ_e = relative mean micropore radius
δ = combined micropore shape and tortuosity factor
η = normalized micropore dimension
ϵ = particle size exponent for mass transfer
θ = porosity, volume fraction
θ_I = volume fraction of the inert phase
Λ = $H_0 \sqrt{e_2{}^0 + \sigma}$
Λ_i = relative mean micropore length
λ = parameter $= \dfrac{a\, k_1 \theta_B{}^0}{k_g{}^0}$
μ_n = relative nth moment
ξ = normalized radius
ρ = apparent density of the solid phase (including inert matter)
ρ_B = apparent density of the solid phase (i.m.f.b.)
ρ_I = density of inert phase
ρ_t = true density of the reacting solid
σ = combination parameter $= \dfrac{S_a{}^0}{S_i{}^0} + \dfrac{\pi k_f\, \rho_t\, r_f{}^2 \bar{l}}{k_1\, M_B\, S_i{}^0}$
τ = dimensionless time $= k_1\, C_g\, M_B\, S_i{}^0\, t$
ϕ = combination rate coefficient (see Part I)
ψ = dimensionless oxidant concentration in particle
ω = weight fraction
Ω_i = relative micropore volume
$\bar{l}$ = micropore length
$\mathcal{D}$ = dimensionless effective diffusivity, $D_e/D_e{}^0$
$\mathcal{R}$ = rate of gasification reaction

Subscripts

A = oxidant
a = macropore property
B = reactive solid
g = bulk phase of gas
I = inert
i = micropore property, radial position
n = order of moment
s = particle external surface
0 = initial condition, particle center
∞ = condition at completion of gasification

Superscripts

0 = initial condition
* = relative parameter
$\bar{\ }$ = mean property [Equation (31)]

LITERATURE CITED

Aris, Rutherford, *Introduction to the Analysis of Chemical Reactors*, p. 128, Prentice-Hall, Englewood Cliffs (1965).

Bankoff, S. G., "Heat Conduction and Diffusion with Change of Phase," in *Adv. Chemical Eng.*, **5**, Academic Press, New York (1964).

Bischoff, K. B., "Accuracy of the Pseudo Steady State Approximation for Moving Boundary Diffusion Problems," *Chem. Eng. Sci.*, **18**, 711 (1963).

Hashimoto, Kenji, and P. L. Silveston, "Gasification-Part 1: Isothermal, Kinetic Control Model For A Solid With A Pore Size Distribution," **19**, 000 (1973a).

———., "Approximation of Rate Expressions Involving Pore Size Distributions," 000 (1973b).

Hills, A. W. D., "The Mechanism of the Thermal Decomposition of Calcium Carbonate," *Chem. Eng. Sci.*, **23**, 297 (1968).

———., "Role of Heat and Mass Transfer in Gas-Solid Reactions Involving Two Solid Phases with Sintering Pellets," in *Heat and Mass Transfer in Process Metallurgy*, p. 40, Inst. Mining and Metallurgy (1967).

Ishida, M., and C. Y. Wen, "Comparison of Kinetic and Diffusional Models for Solid-Gas Reactions," *AIChE J.*, **14**, 311 (1968).

Kawahata, M., and P. L. Walker, Jr., "Mode of Porosity Development in Activated Anthracite," *Proc. 5th Carbon Conf.*, p. 251, Pergamon Press, London (1962).

McGreavy, C., and D. L. Cresswell, "A Lumped Parameter Approximation to a General Model for Catalytic Reactors," *Can. J. Chem. Eng.*, **47**, 583 (1969).

Mingle, J. O., and J. M. Smith, "Effectiveness Factors for Porous Catalysts," *AIChE J.*, **7**, 243 (1961).

Murray, W. D., and F. Landis, "Numerical and Machine Solutions of Transient Heat Conduction Problems Involving Melting or Freezing—Part I," *J. Heat Transfer*, ASME Trans. *81C*, 106 (1959).
Petersen, E. E., *Chemical Reaction Analysis*, Prentice-Hall, Englewood Cliffs (1965).
———, "Reaction of Porous Solids," *AIChE J.*, 3, 443 (1957).
Thomas, W. J., *Carbon*, 3, 435 (1966).
Walker, P. L., Jr., Frank Rusinko, Jr., and L. G. Austin, "Gas Reactions of Carbon" in *Advances in Catalysis*, II, 133, Academic Press, New York (1959).
Wen, C. Y., "Noncatalytic Heterogeneous Solid Fluid Reaction Models," *Ind. Eng. Chem.*, 60, 34 (1963).

Manuscript received April 2, 1971; revision received August 29, 1972; paper accepted October 13, 1972.

The Thermodynamic Approach to Fluidized Drying and Moistening Optimization

STANISLAW SIENIUTYCZ
Institute of Chemical Engineering
Warsaw Technical University
Koszykowa 75, Warsaw, Poland

For drying and moistening processes in batch fluidization and fluidization in a horizontal exchanger, the overall mathematical model describing simultaneous heat and mass exchange is given. On this basis, the problem of finding the optimal temperatures of inlet gas is formulated and investigated for the case when inlet gas humidity is constant. It is explained that when unit economical values of gas and solid phases are linear with regard to unit available energies (exergies), the economical problem of minimum costs is equivalent to the thermodynamical problem of minimum available energy (exergy) dissipation. Therefore, the performance index expression in exergy terms is formulated as a functional of the Bolza form. The dynamic programming method is used to obtain results of optimal trajectories and decisions. The dependence of optimal process time on apparatus price, which is characterized here by a Lagrangian multiplier λ, is pointed out.

The results indicate that the constant gas inlet temperature policy commonly applied to the processes considered here prevents attainment of the process optimum. In fact, increasing inlet temperature until an admissible gas temperature is attained is the optimal policy.

SCOPE

To the class of important processes between gases and granular solids, where the use of variational methods is required for optimization, belong the process of batch fluidization and steady state fluidization process in the horizontal exchanger (Figure 1). In the first process, the solid state changes as a function of time; in the second, it changes as a function of distance when ideal mixing in the first apparatus and ideal mixing in vertical cross-section of the second apparatus is assumed. In an isobaric and adiabatic process, the thermodynamic state of the solid is described by enthalpy I_s and moisture content W_s, the gas by enthalpy i_g and humidity X_g.

In this article the optimal transition of solid phase from one thermodynamic state I_{so},W_{so} to another I_{sk},W_{sk} is considered for the drying or moistening processes shown on Figure 1. This transition occurs during an isobaric and adiabatic process due to simultaneous energy and mass exchange between gas and solid. The total time of such transition is finite.

The usual way of conducting the processes considered is with a constant inlet gas state. In such a case the inlet gas enthalpy i_g and absolute humidity X_g do not change with solid residence time in either of the processes. It is known that driving forces of such processes are large at the beginning and small at the end of the process and that this fact makes the process uneconomical, that is, causes large production costs. Therefore, it should be expected that variable inlet gas states should make the processes considered more economical. The finding of a technique which minimizes production costs is a task of optimization.

It will be shown that in both of the processes considered,